

AttentionMixer: An Accurate and Interpretable Framework for Trustworthy Process Monitoring

Hao Wang *Student Member, IEEE*, Zhiyu Wang, Yunlong Niu, Zhaoran Liu, Haozhe Li, Yilin Liao, Yuxin Huang, Xinggao Liu *Member, IEEE*

Abstract—Trustworthy process monitoring seeks to build an accurate and interpretable monitoring framework, which is critical for ensuring the safety of energy conversion plant (ECP) that operates under extreme working conditions. Current self-attentive token-mixers are inadequate for trustworthy ECP monitoring for two reasons: (1) they rely on step-wise correlations that lack physical semantics in ECP logs, resulting in suboptimal accuracy and ambiguous interpretation; (2) the attention matrix is often cluttered with spurious correlations that obscure meaningful ones, further hindering effective interpretation. To overcome these issues, we propose AttentionMixer, a framework designed to improve the accuracy and interpretability of existing methods and establish a trustworthy ECP monitoring framework. Specifically, to tackle issue (1), we propose to employ a spatial adaptive message passing block that captures variate-wise correlations with meaningful physical semantics. This block is combined with a temporal adaptive message passing block through a mixing operator, resulting in a comprehensive representation of ECP logs that captures both step-wise and variate-wise correlations. To tackle issue (2), we devise a sparse message passing regularizer to eliminate spurious and noisy correlations. We evaluate our proposed framework on two real-world ECP monitoring datasets obtained from the radiation monitoring network for Chinese nuclear power plants, and demonstrate its superior performance in terms of accuracy, interpretability, and overall trustworthiness.

Impact Statement—Energy conversion plants (ECPs) are operating under extreme conditions to improve power conversion efficiency and reduce carbon emissions. Therefore, establishing a trustworthy monitoring framework for ECPs is critical to ensure environmental safety and energy security. However, current solutions such as Convolutional Neural Networks (CNNs), Recurrent Neural Networks (RNNs), and Transformers have limitations in terms of accuracy, interpretability, and trustworthiness. To address these limitations, we propose the AttentionMixer framework to improve the accuracy and interpretability of existing methods and establish a trustworthy ECP monitoring framework. The proposed method's efficacy and superiority are demonstrated

in a large-scale ECP monitoring project: atmospheric nuclear radiation monitoring practice in China. The monitoring logs have been open-sourced on our project website. The proposed framework has the potential to enhance the safety of ECPs by providing a more trustworthy monitoring framework, which is crucial for ensuring environmental safety and energy security.

Index Terms—Artificial intelligence in energy, Time series analysis, Artificial intelligence in security, Artificial intelligence in environment.

I. INTRODUCTION

MONITORING energy conversion plants (ECPs) using high dimensional input sensory data is a critical practice for ensuring energy safety and environmental security. As the demand for power conversion efficiency and carbon emission reduction increases, ECPs are increasingly operating under extreme conditions in order to reach the thermodynamic limit defined by the Clausius theorem. Examples of such extreme operating conditions include the working fluid at extremely high temperatures in coal-based power generation plants [1], the extreme pressure due to the force of falling water in hydroelectric power plants, and the high temperatures and pressures with the risk of nuclear radiation leaks in nuclear power plants [2], [3]. These extreme conditions give rise to severe safety and environmental concerns, highlighting the necessity of a trustworthy monitoring approach for ECPs to ensure energy safety and environmental security.

Trustworthy artificial intelligence (AI) has emerged as a rapidly evolving field that is dedicated to developing safe, interpretable, and transparent AI systems [4]–[7]. The growing concern for AI security has led to the need for trustworthy AI in fundamental domains such as computer vision [8] and natural language processing [9], [10]. We believe such demand is especially salient for ECPs due to the risky and extreme operating conditions. In particular, A trustworthy ECP monitor should therefore possess both high accuracy and interpretability [5]–[7]. The interpretability here refers to the ability of the monitor's decision process to be understood by domain experts, enabling them to verify the correctness based on their own domain knowledge. This is critical for building trust in AI monitors and ensuring the safety of ECPs under extreme operating conditions.

To develop accurate monitors, data-driven approaches have become prevalent [11]–[14] with the development of measurement and learning techniques [15]–[17]. Initially, identification methods like ARIMA [18] and statistical methods such as extreme gradient boosting [19], [20] dominated process monitoring. With the advent of deep learning, deep monitors are

Manuscript received Sept. 28, 2022. This work is supported by the National Natural Science Foundation of China (12075212, 62073288) and Zhejiang University NGICS Platform.

Hao Wang is with the State Key Laboratory of Industrial Control Technology, Hangzhou, CO 310027 China (e-mail: haohaow@zju.edu.cn).

Zhiyu Wang is with the State Key Laboratory of Industrial Control Technology, Hangzhou, CO 310027 China (e-mail: onejoy@zju.edu.cn).

Yunlong Niu is with the State Key Laboratory of Industrial Control Technology, Hangzhou, CO 310027 China (e-mail: nyl0405@zju.edu.cn).

Zhaoran Liu is with the State Key Laboratory of Industrial Control Technology, Hangzhou, CO 310027 China (e-mail: 22032057@zju.edu.cn).

Haozhe Li is with the State Key Laboratory of Industrial Control Technology, Hangzhou, CO 310027 China (e-mail: lihaozhe@zju.edu.cn).

Yilin Liao is with the State Key Laboratory of Industrial Control Technology, Hangzhou, CO 310027 China (e-mail: liaoyl@zju.edu.cn).

Yuxin Huang is with the State Key Laboratory of Industrial Control Technology, Hangzhou, CO 310027 China (e-mail: hxy@zju.edu.cn).

Xinggao Liu is with the State Key Laboratory of Industrial Control Technology, Hangzhou, CO 310027 China (e-mail: lxxg@zju.edu.cn).

This paragraph will include the Associate Editor who handled your paper.

then dominant, with recurrent neural networks (RNN) [12], convolution neural networks (CNN) [21], graph neural networks (GNN) [22]–[24] being the representative approaches, each with its own advantages and limitations. For instance, RNNs can perform lifelong monitoring but are single-threaded; GNNs utilize variate-wise correlations for decision-making but require a predefined adjacency matrix that may be unavailable for ECPs. Recently, self-attentive token-mixers have emerged as a variant of GNNs, which do not require predefined graph structures and have shown great potential in various fields such as computer vision [25] and AI4Science [26]. However, current progress in ECP monitoring is limited to conventional backbones such as CNNs and RNNs, and the huge potential of self-attentive structures remains to be explored.

This paper aims to explore the potential of self-attentive architecture for building a trustworthy ECP monitoring framework. The canonical self-attentive mechanism, however, has inherent characteristics that impede its trustworthiness in ECP monitoring. (1) It only considers step-wise correlations while ignoring variate-wise correlations, which are more informative and relevant for ECP monitoring. Unlike word embeddings, a single step of the monitoring log lacks physical semantics, rendering the step-wise correlations incapable of providing informative interpretations or effective discrimination for ECP monitoring. Therefore, we focus on understanding how the model perceives variate-wise correlations that possess specific physical semantics, rather than step-wise correlations. (2) The generated attention matrix is filled with spurious correlations, which obscures meaningful correlations and further hinders effective interpretation.

To tackle these problems, we propose AttentionMixer under a generalized message passing framework. Specifically, to tackle issue (1), we devise a spatial adaptive message passing (SAMP) block to capture variate-wise correlations with meaningful physical semantics and combine it with a temporal adaptive message passing (TAMP) block using a mixing operator. This produces a comprehensive understanding of ECP logs that captures both step-wise and variate-wise correlations. To tackle issue (2), we devise a sparse message passing regularizer (SMPR) to eliminate spurious correlations and highlight important correlations. By explicitly modeling variate-wise correlations and effectively eliminating spurious correlations, AttentionMixer achieves better accuracy, interpretability, and therefore, trustworthiness in ECP monitoring. To summarize our main contributions:

- We propose AttentionMixer, the first attempt to implement a self-attentive model on both spatial and temporal scales to achieve trustworthy ECP monitoring.
- We develop a sparsification regularizer to eliminate the spurious correlations and improve the accuracy and interpretability of monitoring.
- We conduct extensive experiments on a nuclear power plant monitoring task to demonstrate the trustworthiness of AttentionMixer in ECP monitoring. The real-time monitoring log is open-sourced on our project website¹.

The remaining sections are structured as follows: In Sec-

tion II, we introduce some technical preliminaries to better understand the proposed method. In Section III, we describe the architecture and learning objective of AttentionMixer. In Section IV, we deploy AttentionMixer on a real-world ECP monitoring practice: radiation dose rate monitoring for nuclear power plants, and demonstrate its superiority on trustworthiness. Conclusions and future works are discussed in Section V.

II. PRELIMINARIES

A. Message Passing Mechanism

Message passing is a general framework that encapsulates many spatial GNN models such as GCN, GraphSAGE, and GAT [27]. Let \mathcal{M} and \mathcal{U} be the message generation function and state update function, respectively; the k -th round of message passing for central node ν_i can be expressed as

$$\begin{aligned} m_i^k &= \sum_{\nu_j \in \mathbb{N}_{\mathcal{G}}(\nu_i)} \mathcal{M}(F_i^k, F_j^k), \\ F_i^{k+1} &= \mathcal{U}(m_i^k, F_i^k), \end{aligned} \quad (1)$$

where F_i^k is the feature embedding of ν_i . In (1), \mathcal{M} generates the message embedding m_i^k from the neighboring nodes of ν_i (denoted as $\mathbb{N}_{\mathcal{G}}$), and \mathcal{U} updates the feature embedding of ν_i by fusing the message embedding m_i^k and the original feature embedding F_i^k . Despite its success in many fundamental fields, it is not directly applicable to ECP monitoring due to the lack of graph structure \mathcal{G} .

B. Self-attentive Sequential Models

The self-attentive mechanism [28] can be considered as a form of message passing mechanism, which enables interactions between inputs without prior specification of a graph structure. Let T and D be the number of time steps and the hidden dimension, respectively; $\mathbf{Q} \in \mathbb{R}^{T \times D}$, $\mathbf{K} \in \mathbb{R}^{T \times D}$, and $\mathbf{V} \in \mathbb{R}^{T \times D}$ be the query, key, and value sequences, respectively. The attention matrix is generated as follows:

$$\mathbf{M} = \text{SoftMax}\left(\frac{\mathbf{Q}\mathbf{K}^T}{\sqrt{D}}\right), \quad (2)$$

which is then utilized for fusing the value sequences: $\mathbf{U} = \mathbf{M} * \mathbf{V}$. Notably, (2) can be treated as an message generation and aggregation step in the message passing mechanism, where $\mathbf{U} \in \mathbb{R}^{T \times D}$ corresponds to the message embedding in (1).

The core formula of self-attention mechanism in (2) enables interactions between inputs without requiring a predefined graph, thereby enhancing its flexibility and applicability across various fields. Self-attentive models, beginning with Transformers [28], have revolutionized fundamental domains such as computer vision (e.g., Swin Transformer [25]) and AI for science (e.g., AlphaFold-v2 [26]). Furthermore, self-attentive blocks are increasingly being used as core token-mixers in emerging sequential models, enabling the capture of long-term patterns. For example, FedFormer [29] incorporates a filter-enhanced attentive token-mixer to eliminate data noise; Informer [30] incorporates a ProbSparse self-attention to filter out lazy queries and minimize redundancy; Pyraformer [31] develops a pyramidal attention architecture to capture global

¹<https://data.rmtc.org.cn/gis/PubIndex.html>

and local dependencies at different levels of abstraction in long sequences; LogTrans [32] and TCCT [33] incorporates convolution operators in self-attention block to emphasize the role of locality in generating sequence representation. Meanwhile, some plug-and-play components have been devised to meet task-specific requirements, such as adversarial training to improve multi-step forecast [34] and the patching trick for processing long history [35]. Additionally, some efforts have been made to address the complexity of self-attentive models with ultra-long input sequences, with notable examples being Reformer [36], BigBird [37], and PerFormer [38].

Self-attentive models have shown promise in many disciplines that feature sequential modeling. However, current implementations are based on step-wise correlations that are insufficient for providing informative interpretations or effective discrimination for ECP monitoring. In this study, we propose a self-attentive approach that captures both variate-wise and step-wise correlations, thus addressing the aforementioned issues and highlighting the role of self-attentive mechanisms in constructing trustworthy ECP monitors.

III. METHODOLOGY

In this section, we introduce AttentionMixer, which is based on a generalized message passing paradigm as described in Section II-A. AttentionMixer utilizes the spatial adaptive message passing (SAMP) block to capture the correlations between variates and the temporal adaptive message passing (TAMP) block to capture the correlations between time steps. Additionally, AttentionMixer incorporates a sparse message passing regularizer (SMPR) to eliminate spurious correlations without the need for unstable sampling procedures. The technical distinctions from prevalent self-attentive methods involve: (1) the depiction of variate-wise correlations; (2) the elimination of spurious relationships.

A. Problem Definition

We use bold uppercase letters (*e.g.*, \mathbf{X}) to denote matrix, lowercase letters (*e.g.*, \mathbf{x}) to denote associated vectors. The input variables at the t -th step is denoted as $\mathbf{x}_t \in \mathbb{R}^{D \times 1}$. Given historical observations $\mathbf{X}_t := [\mathbf{x}_{t+1}, \mathbf{x}_{t+2}, \dots, \mathbf{x}_{t+T}]$ with window length T , our goal is to learn a function $f: \mathbb{R}^{T \times D} \rightarrow \mathbb{R}$ such that $f(\mathbf{X}_t) \rightarrow y_t^H$, where y_t^H is the value of key performance indicators (KPIs) at the $t + T + H$ step.

In the offline training stage, we aim to accurately forecast KPIs using historical KPIs and external factors [12], [13]; in the inference stage, we anticipate that anomalous events will be indicated by large deviations between actual and forecast KPI values, as the training set only consists of normal logs.

B. Spatial Adaptive Message Passing Module

Canonical self-attention methods [28] treat each time step as a node and perform message passing at a temporal scale. This approach neglects variate-wise correlations and thus results in suboptimal accuracy and hinders meaningful interpretation in ECP monitoring. To address this issue, the SAMP module in this section depicts variate-wise correlations by performing

message passing at a spatial scale, with each variate being treated as a node. Figure 1 (b) shows the k -th round of message passing with input $\mathbf{S}^{k,\text{in}} \in \mathbb{R}^{D \times T}$ and output $\mathbf{S}^{k,\text{out}} \in \mathbb{R}^{D \times T}$. The computation workflow comprises three steps as follows.

1) *Message Generation*: We first generate the outgoing message embeddings $\mathbf{V}_S^k \in \mathbb{R}^{D \times T}$ for each node by feeding their individualized state embeddings into a multiple layer perception (MLP) layer:

$$\mathbf{V}_S^k := \text{MLP}(\mathbf{S}^{k,\text{in}}), \quad (3)$$

where $\mathbf{V}_S^k[i] \in \mathbb{R}^T$ is the outgoing message embedding of the i -th node, the MLP layer involves a learnable affine transformation and a linear activation function following [28]. We then define an attention matrix $\mathbf{M}_S^k \in \mathbb{R}^{D \times D}$ as follow:

$$\begin{aligned} \mathbf{Q}_S^k &:= \text{MLP}(\mathbf{S}^{k,\text{in}}), \\ \mathbf{K}_S^k &:= \text{MLP}(\mathbf{S}^{k,\text{in}}), \\ \hat{\mathbf{M}}_S^k &:= \mathbf{Q}_S^k * [\mathbf{K}_S^k]^T / \sqrt{D}, \\ \mathbf{M}_S^k &:= \text{SoftMax}(\hat{\mathbf{M}}_S^k), \end{aligned} \quad (4)$$

where $\mathbf{M}_S^k[i, j]$ is a generalized similarity measure between the i -th node and the j -th node; the division of \sqrt{D} avoids numerical errors during optimization [28]. The SoftMax operation normalizes the attention scores of each node as follow:

$$\mathbf{M}_S^k[i, j] := \frac{\exp(\hat{\mathbf{M}}_S^k[i, j])}{\sum_{i=1}^D \exp(\hat{\mathbf{M}}_S^k[i, j])}. \quad (5)$$

Finally, we generate the incoming message embeddings $\mathbf{U}_S^k \in \mathbb{R}^{D \times T}$ for each node by aggregating the outgoing message embeddings using the attention matrix \mathbf{M}_S^k . The main intuition here is straightforward: neighbors with more remarkable similarities should convey more important messages. As such, the incoming message embeddings are calculated as

$$\mathbf{U}_S^k := \mathbf{M}_S^k * \mathbf{V}_S^k, \quad (6)$$

where the incoming message embedding of the i -th node is a weighted sum of the outgoing message embeddings of its neighbors, with the weight being its attention to its neighbors:

$$\mathbf{U}_S^k[i, :] := \sum_{j=1}^D \mathbf{M}_S^k[i, j] \mathbf{V}_S^k[j, :]. \quad (7)$$

2) *State Update*: The state embedding for each node is renewed according to its previous state embedding $\mathbf{S}^{k,\text{in}}$ and incoming message embedding \mathbf{U}_S^k as follow:

$$\mathbf{S}^{k,\text{out}} := \text{LayerNorm}(\mathbf{S}^{k,\text{in}} + \mathbf{U}_S^k), \quad (8)$$

where the residual link preserves the previous state embeddings that is excluded in the generation process of \mathbf{U}_S^k ; the LayerNorm technique standardizes the data distribution at each layer to stabilize the training process.

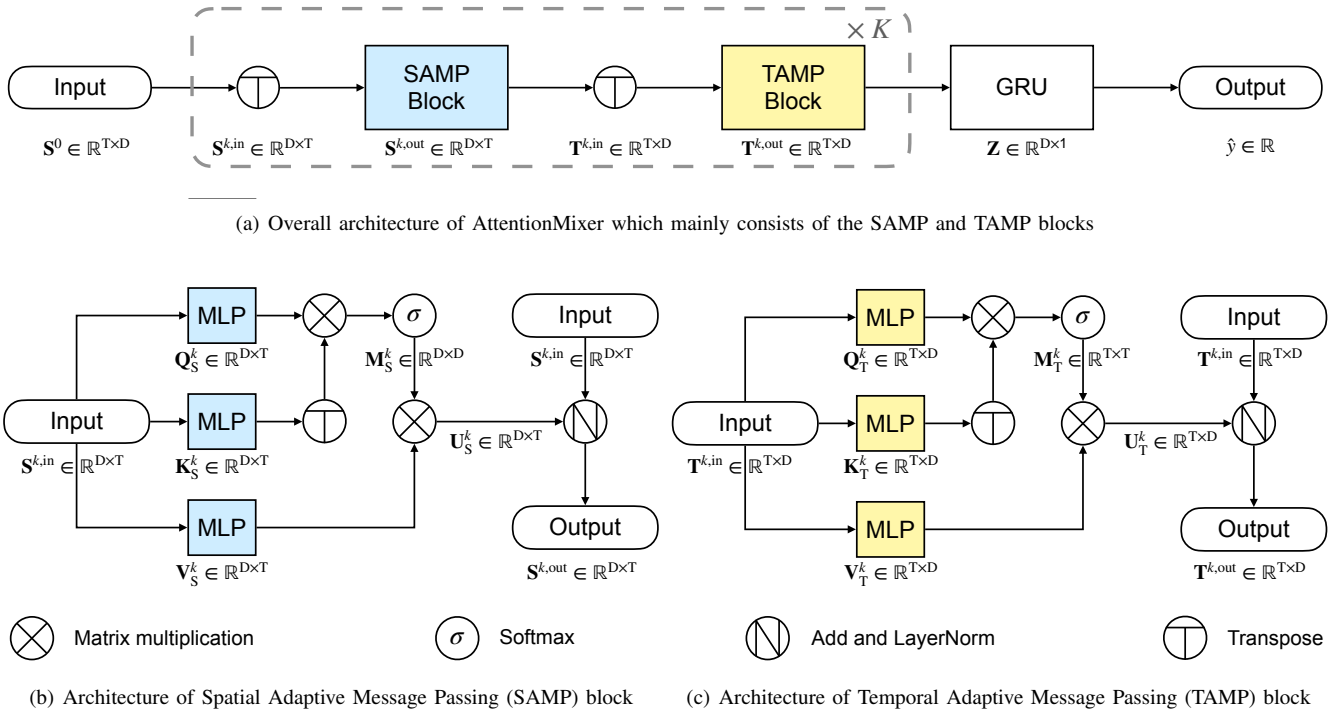


Fig. 1. Overview of the architecture of AttentionMixer, where the output of each module is marked under the corresponding module.

C. Temporal Adaptive Message Passing Module

The SAMP module focuses on variate-wise correlations while ignoring temporal correlations. However, temporal correlations are crucial for capturing auto-regressive characteristics in monitoring logs. Thus, ignoring temporal correlations can result in suboptimal performance for ECP monitoring, necessitating the TAMP module in this section.

Figure 1 (c) illustrates the k -th round of temporal message passing, with $\mathbf{T}^{k,\text{in}} \in \mathbb{R}^{T \times D}$ representing the input and $\mathbf{T}^{k,\text{out}} \in \mathbb{R}^{T \times D}$ representing the output. The computation workflow is similar to that of SAMP, but TAMP relies on correlations between time steps rather than variates. TAMP models such step-wise correlations by performing message passing at a temporal scale, with each time step being treated as a node and the input $\mathbf{T}^{k,\text{in}}$ serving as the state embeddings of T nodes. The message passing route $\mathbf{M}_T^k \in \mathbb{R}^{T \times T}$ thus depends on the correlations between time steps.

D. Sparse Message Passing Regularizer

The correlations learned by self-attentive models are highly dense according to Figure 7 (a), whereas the actual relationships in the physical world are sparse, as per the Occam's razor principle [39], [40]. This implies the existence of many spurious relationships, which can lead to overfitting and obscure meaningful relationships [37], ultimately compromising the accuracy and interpretability of monitoring. To address this issue, several graph sparsification techniques [24], [30], [41] have been proposed to obtain interpretable and meaningful graph structures. However, most of these techniques rely on sampling, resulting in significant variance in both training and inference phases, which is undesirable for ECP monitoring under extreme working conditions.

To avoid introducing sampling during model inference, regularization on the graph structure during the training process is preferable. In our framework, the graph structure is represented by the message passing route \mathbf{M} , and a natural approach is to regularize their ℓ_1 norm as follows:

$$\mathcal{L}_{\text{smpr}} := \sum_{k=1}^K \|\mathbf{M}_S^k\|_1 + \sum_{k=1}^K \|\mathbf{M}_T^k\|_1, \quad (9)$$

$$\|\mathbf{M}_S\|_1 := \sum_{i,j=1}^D |\mathbf{M}_S[i,j]|, \quad \|\mathbf{M}_T\|_1 := \sum_{i,j=1}^T |\mathbf{M}_T[i,j]|$$

where $\|\cdot\|_1$ indicates the mean absolute value of the matrix, which promotes sparse solutions during model training. This regularization approach helps eliminate spurious relationships and highlight meaningful relationships, ultimately improving the accuracy and interpretability of process monitoring.

E. AttentionMixer Framework for ECP Monitoring

1) *Overall Architecture*: As depicted in Figure 1 (a), AttentionMixer consists of cascaded SAMP and TAMP blocks. The preprocessed data is first fed into SAMP, *i.e.*, $\mathbf{S}^{1,\text{in}} = \mathbf{S}^0$, where messages are passed through the adaptive spatial graph. Next, the output of SAMP undergoes a transposition operation to obtain the input for TAMP. Specifically, the spatial and temporal dimensions of SAMP's output are transposed to get the input to TAMP:

$$\begin{aligned} \mathbf{S}^{k,\text{out}} &:= \text{SAMP}(\mathbf{S}^{k,\text{in}}), \\ \mathbf{T}^{k,\text{in}} &:= \text{Transpose}(\mathbf{S}^{k,\text{out}}), \end{aligned} \quad (10)$$

where $k \leq K$ is the round of current message passing. Afterwards, TAMP extracts the temporal correlations in the

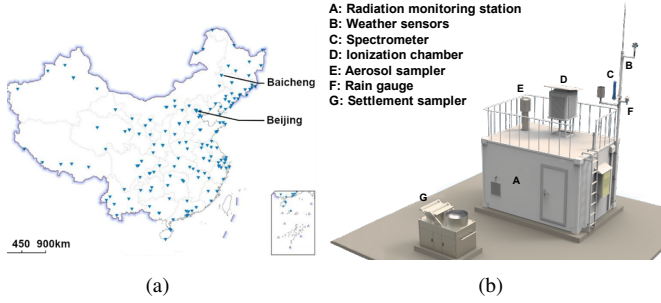


Fig. 2. Overview of the national automatic nuclear radiation monitoring network in China: (a) the distribution of monitoring stations that have been deployed; (b) the composition of a specific monitoring station.

data, and the transpose of its output is the input to the SAMP block in the next round of message passing:

$$\begin{aligned} \mathbf{T}^{k,\text{out}} &:= \text{TAMP}(\mathbf{T}^{k,\text{in}}), \\ \mathbf{S}^{k+1,\text{in}} &:= \text{Transpose}(\mathbf{T}^{k,\text{out}}). \end{aligned} \quad (11)$$

The output of the last TAMP block, $\mathbf{T}^{K,\text{out}}$, is fed into a gated recurrent unit (GRU) decoder to get the dose rate estimate:

$$\mathbf{Z} := \text{GRU}(\mathbf{T}^{K,\text{out}}), \quad \hat{y}_t^H := \text{Linear}(\mathbf{Z}), \quad (12)$$

where \hat{y}_t^H is the output of AttentionMixer, H is the forecast horizon, $\text{Linear}(\cdot)$ is a MLP-layer with linear activation.

2) *Learning Objective*: The learning objective aims to minimize the error of forecast and the density of message passing. Given input \mathbf{X}_t and label y_t^H , the forecast error is

$$\mathcal{L}_{\text{pred}} := (y_t^H - \hat{y}_t^H)^2, \quad (13)$$

where y_t^H is the actual radiation dose rate at the $t + H$ time step, \hat{y}_t^H is the output of the proposed AttentionMixer given input $\mathbf{S}^0 := \mathbf{X}_t$. The overall learning objective is

$$\mathcal{L}_{\text{Mixer}} = \mathcal{L}_{\text{pred}} + \lambda \cdot \mathcal{L}_{\text{smpr}}, \quad (14)$$

where λ controls the strength of SMPR. The network structure and learning objective cooperate to improve accuracy and interpretability, both critical for nuclear radiation monitoring.

IV. EXPERIMENTS

To demonstrate the effectiveness of the proposed AttentionMixer for ECP monitoring under extreme working conditions, we conduct experiments on the nuclear radiation monitoring downstream task, where the monitoring logs are collected from real-world monitoring stations for nuclear power plants.

A. Background of Nuclear Radiation Monitoring

As a resilient and reliable source of energy [42], [43], nuclear power plants generate nearly 800 billion kilowatt-hours of electricity per year in America, supplying more than 60% of the emission-free electricity, reducing about 500 million metric tons of carbon emission [44]. However, as an extreme-condition ECP, it raises serious concerns regarding environmental safety and energy security [2], [3]. In the event of a nuclear anomaly, excessive amounts of radionuclides can be released into the atmosphere, causing severe environmental

TABLE I
VARIABLE DEFINITION OF THE MONITORING LOG

Field	Unit of measure
Atmospheric radiation	
Dose rate	nGy / h
Spectrum (1024 channels)	ANSI/IEEE N42.42
Meteorological conditions	
Temperature	°C
Humidity	%
Atmosphere pressure	hPa
Wind direction	Clockwise angle
Wind speed	m / s
Precipitation indicator	Boolean value
Amount of precipitation	mm
Spectrometer operating conditions	
Battery voltage	V
Spectrometer voltage	V
Spectrometer temperature	°C

pollution. As a preventive technology, automatic monitoring networks for nuclear power plants have been widely deployed, such as the RadNet in America [45], the Fixed Point Surveillance network in Canada [46], and the Atmospheric Nuclear Radiation Monitoring Network (ANRMN) in China.

The ANRMN project consists of approximately 500 individual stations for nuclear radiation monitoring, as shown in Figure 2. The key performance indicator (KPI) of these stations is the γ -ray dose rate in the atmosphere [47], which reflects the intensity of radionuclides. However, the measured dose rate is not only related to the intensity of generated radionuclides but also affected by meteorological conditions and spectrometer operating conditions [48], [49]. For example, natural radionuclide radon in the air can be washed to the ground during rainfall, resulting in a spurious increase in the dose rate measured by monitoring sensors [48]. Ignoring such external factors can lead to false alarms and reduced reliability of monitoring.

To construct data-driven ECP monitoring system, the monitoring log includes atmospheric radiation data, meteorological conditions, and spectrometer operating conditions. The atmospheric radiation data is collected with the ionization chamber and spectrometer in Figure 3. The ionization chamber measures γ -ray dose rate [50], and its measurements are uploaded daily on our online monitoring board². The spectrometer³ measures spectrum, an important indicator of radionuclide concentrations in the environment. Figure 4 (a) shows a 1024-channel spectrum where different channels show different patterns of variation, with the energy decaying in higher channels. Figure 4 (b) provides further details on the dynamics of the measured spectrum with four selected channels, which are non-stationary and noisy due to the influence of external factors. In order to calibrate such external impacts, meteorological conditions (*e.g.*, precipitation) and spectrometer operating conditions (*e.g.*, battery voltage) are supplemented in the monitoring logs.

²Real-time dose rate data has been released on [our website](#).

³The spectrometer employs the SARA detector by ENVINET GmbH.

TABLE II
DESCRIPTION OF SAMPLING STRATEGY.

Station	Location	#Sample	#Variable	Interval	Start time
Changchi	Beijing	38,686	1,034	5 min	10/3/2020
Industrial Park	Baicheng	38,687	1,034	5 min	21/4/2020

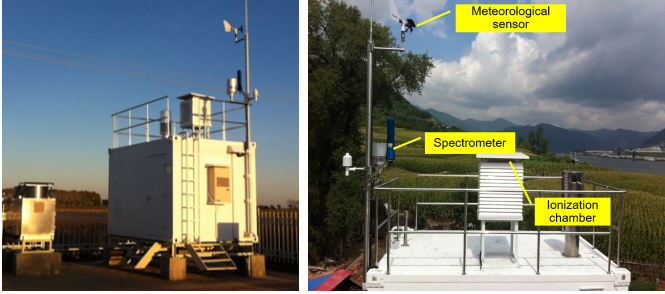


Fig. 3. Real-world monitoring stations with key sensors being highlighted.

B. Experimental Setup

1) *Datasets*: Two industrial benchmarks are constructed using the monitoring logs obtained from the ANRMN project. These benchmarks consist of 1034 input variables, as described in Table I, which includes the 1024-channel spectrum, 7-channel meteorological conditions, and 3-channel spectrometer operating conditions. The sampling strategy used to create both benchmarks is detailed in Table II. Both benchmarks are divided chronologically into training, validation, and test sets in a ratio of 0.7:0.15:0.15. Finally, they are scaled using a min-max scaler to facilitate model training and evaluation.

2) *Baselines*: AttentionMixer is compared with three groups of baselines. (1) Identification-based models: Auto-Regression (AR) [18], Moving Average (MA) [18], AutoRegressive Integrated Moving Average (ARIMA) [18]; (2) Statistic-based models: Lasso Regression (LASSO) [51], Support Vector Regression (SVR) [20], Random Forest (RF) [52], Gradient Boosting Decision Tree (GBDT) [19], eXtreme Gradient Boosting (XGB) [19]; (3) Deep models: Long Short-Term Memory (LSTM) [53], Gated Recurrent Unit (GRU) [54], Transformer [28], Informer [30], FedFormer [29]. Consistent with AttentionMixer, we use GRU as the decoder for former-like baselines for fair comparison.

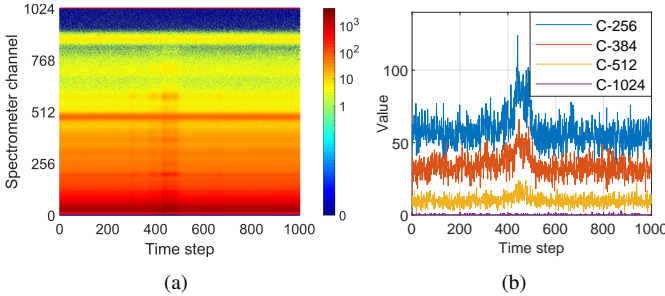


Fig. 4. Spectrometer measurements and dose rates of 1000 sequential time steps starting from 2020/5/15 21:54:00, in Baicheng Station, Jilin.

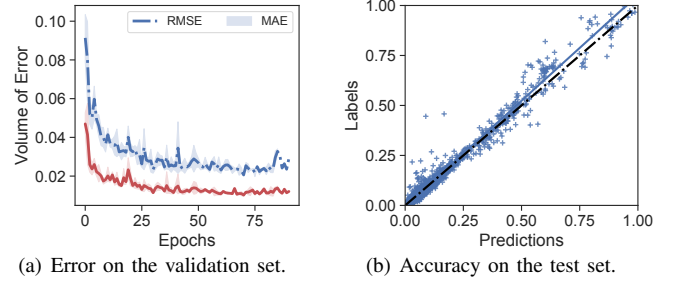


Fig. 5. Monitoring performance of AttentionMixer on Beijing benchmark.

3) *Training Strategy*: In our experiments, all deep models are trained for a total of 200 epochs using the Adam optimizer [55] with early stopping strategy. The batch size is set to 64, and the window length T is set to 16. The learning rate is set to 0.001, and the patience for early stopping is set to 15 epochs. The strength λ of SMPR is set to $5e^{-5}$ for the Baicheng station and $1e^{-5}$ for the Beijing station, respectively. The round K of message passing is set to 2. To ensure a fair comparison, we applied this setup to all methods. We check-point models on the validation set every epoch, and report the best performance on the test set.

4) *Evaluation Strategy*: The coefficient of determination (R^2) is used as the main fitness metric in line with [22], [23].

$$R^2 = 1 - \frac{\sum_{t=1}^N (y_t^H - \hat{y}_t^H)^2}{\sum_{i=1}^N (y_t^H - \bar{y}_t^H)^2}, \quad (15)$$

where y_t^H is the actual dose rate, \hat{y}_t^H is the estimated dose rate, \bar{y}_t^H is the mean value of y_t^H for $t = 1 : N$, N is the size of test set. To provide a comprehensive model comparison, root mean squared error (RMSE) and mean absolute error (MAE) are employed as additional metrics:

$$\begin{aligned} \text{RMSE} &= \left[\frac{1}{N} \sum_{t=1}^N (y_t^H - \hat{y}_t^H)^2 \right]^{1/2}, \\ \text{MAE} &= \frac{1}{N} \sum_{t=1}^N |y_t^H - \hat{y}_t^H|. \end{aligned} \quad (16)$$

C. Overall Performance

Table III compares AttentionMixer and its competitors at four forecast horizons ($H = 1, 3, 5, 7$). The observations can be summarized as follows:

Identification-based models demonstrate practical short-term forecasting capabilities. For example, ARIMA achieves an R^2 of 0.77 and 0.79 on the Beijing and Baicheng benchmarks, respectively, confirming the presence of autocorrelation characteristics in the data. However, these models are limited to describing linear autocorrelation, making them vulnerable to non-linear autocorrelation in datasets. This limitation becomes evident in the long-term forecast performance, where ARIMA achieves an R^2 of 0.73 for $H=7$ on the Beijing benchmark but only 0.12 on the Baicheng benchmark. This significant drop is attributed to the strong non-linear autocorrelation in the Baicheng benchmark.

TABLE III
COMPARATIVE STUDY ON THE BEIJING AND BAICHENG BENCHMARKS OVER FOUR FORECAST HORIZONS.

Methods		Metrics	Beijing Station				Baicheng Station				
			H=1	H=3	H=5	H=7	H=1	H=3	H=5	H=7	
Identification based models	AR	MAE	0.0925	0.1005	0.1068	0.1161	0.0999	0.1329	0.1669	0.1899	
		R ²	0.7672	0.7265	0.6887	0.6455	0.7051	0.5110	0.2196	-0.0282	
	MA	MAE	0.0952	0.1027	0.1081	0.1161	0.1537	0.1794	0.2019	0.2201	
		R ²	0.7563	0.7193	0.6828	0.6437	0.3457	0.1095	-0.1363	-0.3642	
	ARIMA	MAE	0.0962	0.0982	0.1048	0.1000	0.0818	0.1094	0.1452	0.1762	
		R ²	0.7700	0.7339	0.7228	0.7342	0.7954	0.6611	0.3940	0.1258	
Statistic based models	LASSO	MAE	0.0500	0.0511	0.0527	0.0546	0.0207	0.0210	0.0216	0.0224	
		R ²	0.4015	0.3663	0.3124	0.2491	0.3998	0.3708	0.3260	0.2719	
	SVR	MAE	0.0723	0.0712	0.0677	0.0664	0.0486	0.0599	0.0647	0.0655	
		R ²	0.4743	0.4843	0.4828	0.4429	0.3247	-0.0073	-0.2074	-0.2936	
	RF	MAE	0.0337	0.0360	0.0383	0.0413	0.0159	0.0171	0.0172	1.0183	
		R ²	0.8580	0.8193	0.7589	0.6753	0.8918	0.8393	0.7879	0.7118	
	GBDT	MAE	0.0396	0.0406	0.0420	0.0444	0.0176	0.0175	0.0178	0.0183	
		R ²	0.7453	0.7137	0.6543	0.5678	0.7840	0.7559	0.7057	0.6460	
	XGB	MAE	0.0302	0.0332	0.0370	0.0412	0.0105	0.0118	0.0136	0.0149	
		R ²	0.8943	0.8393	0.7684	0.6719	0.9485	0.9012	0.8335	0.7555	
	Deep models	LSTM	MAE	0.0181	0.0214	0.0251	0.0294	0.0160	0.0170	0.0183	0.2000
			R ²	0.9025	0.8343	0.7478	0.6547	0.8916	0.8331	0.7640	0.6886
GRU		MAE	0.0177	0.0214	0.0247	0.0280	0.0179	0.0189	0.0198	0.0210	
		R ²	0.9021	0.8382	0.7577	0.6742	0.8621	0.8046	0.7426	0.6720	
Transformer		MAE	0.0142	0.0223	0.0282	0.0334	0.0111	0.0154	0.0177	0.0210	
		R ²	0.9642	0.8640	0.7915	0.6826	0.9423	0.7996	0.7318	0.6252	
Informer		MAE	0.0189	0.0287	0.0276	0.0482	0.0123	0.0140	0.0221	0.0186	
		R ²	0.9082	0.8444	0.7745	0.6144	0.8949	0.8416	0.6941	0.6738	
Fedformer		MAE	0.0104	0.0185	0.0233	0.0254	0.0069	0.0100	0.0125	0.0149	
		R ²	0.9750	0.9239	0.8506	0.7684	0.9765	0.9215	0.8483	0.7882	
Current work		AttentionMixer	MAE	0.0104	0.0197	0.0213	0.0280	0.0066	0.0093	0.0112	0.0156
			R ²	0.9756	0.9044	0.8465	0.7245	0.9783	0.9229	0.8708	0.7859

Bold fonts and underlined fonts indicate the best and second best performance for each metric, respectively.

Statistic-based models incorporate external factors such as meteorological and spectral measures, leading to competitive short-term forecast performance. Non-linear estimators (RF, GBDF, XGB) with higher capacity outperform linear estimators (LASSO, SVR). For example, RF exhibits a MAE of 0.033 and 0.0159, significantly outperforming LASSO and SVR. Additionally, XGB shows remarkable performance, surpassing conventional deep models like LSTM and GRU on both datasets. This can be attributed to XGB's ability to capture effective intersections between input variables in tabular datasets, enabling it to outperform some deep models when variate-wise intersections dominate the task. These findings highlight the importance of effectively modeling variate-wise intersections to improve the accuracy of ECP monitoring.

Deep models achieve the best overall performance among all baselines. RNN-based deep models, such as LSTM and GRU, outperform all non-deep models except XGB. Self-attentive models further enhance monitoring performance significantly, indicating their potential for ECP monitoring, although more exploration is needed. Notably, Informer is inferior to Transformer in our context, possibly due to the overly aggressive and restrictive sampling-based sparsification strategy, which can reduce model performance. A similar phenomenon is observed in AttentionMixer, where overly large strength of SMPR can lead to a decrease in performance.

AttentionMixer outperforms all baseline methods on most metrics and benchmarks. By explicitly modeling variate-wise

correlations and effectively eliminating spurious correlations, AttentionMixer achieves higher accuracy. A notable strong baseline is FedFormer, which achieves competitive performance with AttentionMixer. However, FedFormer fails to consider variate-wise correlations, and its decision process lacks interpretability, which hinders its trustworthiness in ECP monitoring under extreme working conditions.

Figure 5 provides a more detailed demonstration of AttentionMixer's monitoring performance. During the training phase, the model converges rapidly, as evidenced by the validation error stabilizing after approximately 25 epochs. In the test phase, AttentionMixer accurately estimates dose rates, as indicated by the distribution of estimated and actual values clustering around a line with a slope of 1.

D. Discussion on Trustworthiness

1) *Accuracy*: A trustworthy ECP monitoring framework should be accurate. To assess the effectiveness of AttentionMixer's components in improving accuracy, we compare its performance with four variants:

- 1) w/o SAMP: AttentionMixer without the SAMP module;
- 2) w/o TAMP: AttentionMixer without the TAMP module;
- 3) w/o SMPR: AttentionMixer without SAMP, *i.e.*, $\lambda = 0$;
- 4) w/o asymmetry: AttentionMixer with undirected message passing graph, *i.e.*, $\mathbf{Q}_S^k = \mathbf{K}_S^k$ and $\mathbf{Q}_T^k = \mathbf{K}_T^k$.

The results in Table IV reveal the observations as follows. First, both SAMP and TAMP modules are crucial for achieving

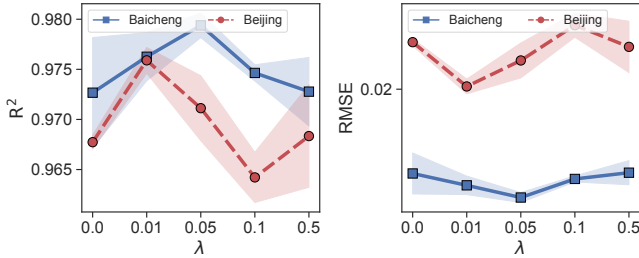
TABLE IV
COMPARISON OF ATTENTIONMIXER AND ITS VARIANTS (MEAN±STD).

Dataset	Beijing Station			Baicheng Station		
	RMSE ↓	MAE ↓	R ² ↑	RMSE ↓	MAE ↓	R ² ↑
w/o SAMP	0.0572±0.0025 [†]	0.0315±0.0034 [†]	0.8066±0.0167 [†]	0.0339±0.0008 [†]	0.0155±0.0007 [†]	0.8413±0.0074 [†]
w/o TAMP	0.0234±0.0009 [†]	0.0124±0.0008 [†]	0.9676±0.0025 [†]	0.0145±0.0009 [†]	0.0085±0.0004 [†]	0.9710±0.0036 [†]
w/o SMPR	0.0240±0.0012 [†]	0.0118±0.0003 [†]	0.9660±0.0036 [†]	0.0141±0.0019	0.0073±0.0008	0.9723±0.0070 [†]
w/o asymmetry	0.0209±0.0021	0.0104±0.0008	0.9739±0.0052	0.0137±0.0013	0.0069±0.0004	0.9740±0.0052 [†]
AttentionMixer	0.0203±0.0008	0.0104±0.0005	0.9756±0.0019	0.0125±0.0008	0.0066±0.0003	0.9783±0.0027

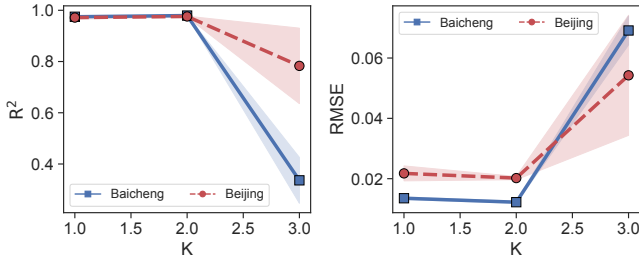
* marks the variants significantly inferior to AttentionMixer at p-value< 0.05 over paired sample t-test. Bolded fonts indicate the best results.

TABLE V
COMPLEXITY ANALYSIS OF FOUR BLOCKS

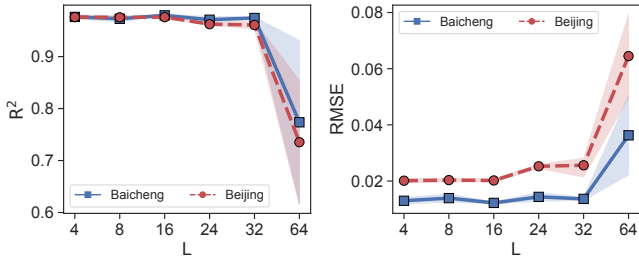
Blocks	Complexity	Sequential Ops	Path Length
RNN	$\mathcal{O}(T \cdot D^2)$	$\mathcal{O}(T)$	$\mathcal{O}(T)$
TCN	$\mathcal{O}(\tau \cdot T \cdot D^2)$	$\mathcal{O}(1)$	$\mathcal{O}(\log_{\tau} T)$
TAMP	$\mathcal{O}(T^2 \cdot D)$	$\mathcal{O}(1)$	$\mathcal{O}(1)$
SAMP	$\mathcal{O}(T \cdot D^2)$	$\mathcal{O}(1)$	$\mathcal{O}(1)$



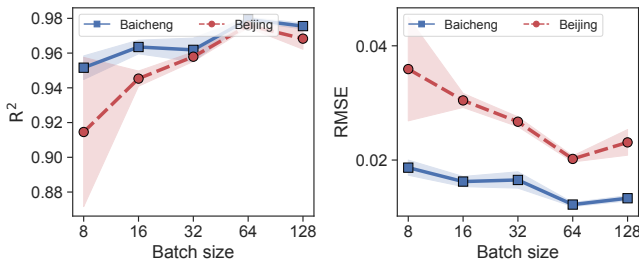
(a) Performance with different strengths of SMPR λ ($\times 10^{-2}$).



(b) Performance with different rounds of message passing K.



(c) Performance with different settings of window length L.



(d) Performance with different settings batch size.

Fig. 6. Parameter sensitivity studies of AttentionMixer, where the marker and dark area indicates the mean value and 90% confidence interval, respectively.

overall performance, emphasizing the significance of variant-wise and step-wise correlations in accurate ECP monitoring.

Second, the SMPR mechanism, which eliminates noisy correlations and reduces overfitting risks, significantly improves AttentionMixer's performance. For instance, it enhances R² from 0.966 to 0.975 on the Beijing benchmark and reduces RMSE from 0.014 to 0.012 on the Baicheng benchmark.

Finally, inclusion of asymmetry in attention matrices also contributes to improved performance. Notably, in a temporal scale, the latter step is a consequence of the former step, but not vice versa; in a spatial scale, meteorological conditions affect dose-rate measures, but not vice versa. Hence, asymmetry exists in nuclear radiation monitoring logs, and disregarding this property diminishes model accuracy.

2) *Interpretability*: Interpretability and consistency with expert knowledge are crucial for trusting AI monitors in extreme operating conditions. However, most existing monitoring solutions lack interpretability: conventional deep models such as RNNs and TCNs consist of stacked non-linear transformations that lack physical meaning; canonical self-attention methods rely on step-wise correlations, which have no specific semantic in ECP logs and are not understandable by human experts.

To address this limitation, we introduce the SAMP block, which explicitly models variate-wise correlations and enables a transparent decision process as per Figure 7. Unlike step-wise attention, sequence-wise correlation contains more discriminative information and has understandable physical meaning in the context of ECP monitoring. This technical advancement is significant not only for ECP monitoring but also for other fields like natural language processing and time series forecast.

Furthermore, the attention matrix generated by AttentionMixer is highly dense, as depicted in Figure 7 (a). However, real-world relationships are often sparse. The dense attention matrix contains spurious correlations that obscure meaningful ones, reducing interpretability. By involving SMPR, the attention matrix gradually becomes sparsified and spurious re-

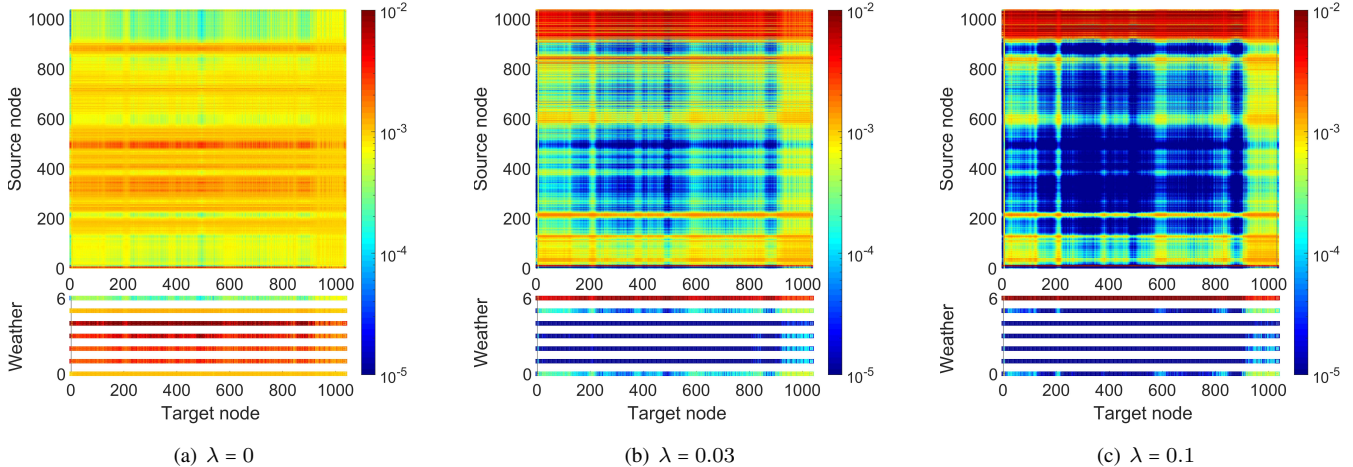


Fig. 7. The attention matrix in the first SAMP module with different strengths of SMPR λ .

relationships are eliminated, as demonstrated in the dark red part of Figure 7 (b-c). Consequently, the meaningful relationships are highlighted, and the model’s interpretability is improved.

Moreover, the interpretation of AttentionMixer can be validated with existing expert knowledge. The lower half of Figure 7 illustrates the impact of weather conditions on other measurements, where the sixth weather condition (precipitation) has a significant impact on most spectrometer measures. Increasing the strength of SMPR further emphasizes this phenomenon. Expert knowledge [47], [48] confirms that precipitation and spectrometer measures are mechanically related, as rain washes radionuclide radon in the air to the ground, leading to an increase in spectrometer measures. This finding highlights the consistency of our monitoring process with expert knowledge, which is critical for trusting AI monitors in extreme-condition ECPs.

E. Parameter Sensitivity Study

In this section, we aim to examine four critical hyperparameters that can significantly affect the final performance of our model. These hyperparameters include the strength of SMPR (λ), the round of message passing (K), the window length (L), and the batch size.

The strength of SMPR (λ) is a crucial hyperparameter that directly affects the learning objective (14) and, consequently, has a significant impact on the final performance. As shown in Figure 6, SMPR positively contributes to the overall monitoring performance within a wide range of λ values. Specifically, the value of R^2 increases from 0.968 at $\lambda = 0$ to 0.976 at $\lambda = 0.0001$. However, assigning a large weight to SMPR can have a detrimental effect on the performance, with R^2 dropping to 0.969 at $\lambda = 0.005$. It is speculated that over-emphasizing SMPR in a multitask learning framework could make it challenging to minimize forecast errors effectively.

The round of message passing (K) is another crucial hyperparameter. According to Figure 6, a single round of message passing is adequate to obtain a comprehensive spatio-temporal representation, which can be effectively utilized for monitoring. Incorporating additional rounds of message passing

provides limited benefits and may even lead to overfitting and optimization difficulties, resulting in performance drop.

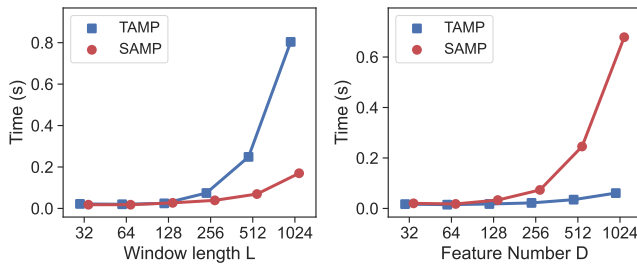
We further investigate the impact of window length (L) on performance. Overall, the model’s performance is relatively insensitive to this parameter within a larger range, indicating that modeling overly long-term step-wise relationships is unnecessary for effective monitoring. Rather, establishing effective variate-wise relationships is crucial for achieving good monitoring performance. These findings align with the conclusions drawn from our ablation studies in Table IV. Finally, we investigate the effect of batch size on performance. Overall, larger batch sizes can stabilize the training process and improve the final results within a wide range.

F. Complexity Analysis

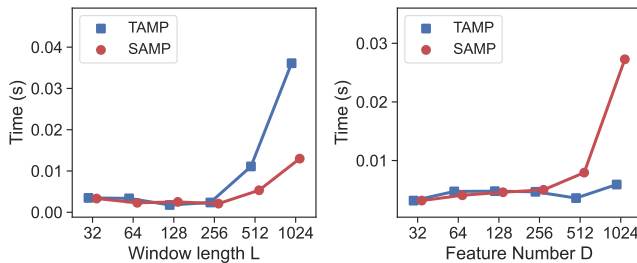
In this section, we provide a comparison of computational costs among different sequence transformation methods, as reported in Table V following [28]. The methods are employed to transform one sequence ($\mathbf{x}_1, \dots, \mathbf{x}_T$) to another sequence ($\mathbf{z}_1, \dots, \mathbf{z}_T$) with equal length T and feature number D . Three metrics are considered, including complexity, sequential ops, and path length, which respectively measure the amount of floating-point operations, non-parallelizable operations, and the minimum number of layers to model the relationships between any time steps.

RNNs exhibit inefficiencies in training and inference due to sequential operations and path length. TCNs, with a kernel length τ , allow for full parallelization; however, the need to stack multiple TCN layers to model global relationships limits efficiency for long-term dependencies. TAMPs, specifically the vanilla self-attention block, demonstrate advantages in terms of parallelization and path length, but their complexity of $\mathcal{O}(T^2)$ poses challenges in handling large window length [37], [56]. The proposed SAMP module enjoys the superiority of parallelization and path length while reducing the complexity to $\mathcal{O}(T)$ in relation to window length.

Figure 8 depicts the inference time of the SAMP and TAMP modules for 64 samples, indicating that the inference time



(a) Inference time on the Intel(R) Xeon(R) Gold 6140 CPU.



(b) Inference time on the Nvidia RTX Titan GPU.

Fig. 8. Inference time of the SAMP and TAMP blocks on CPUs (a) and GPUs (b). The default settings of L and D are 16 and 32, respectively. The batch size is set to 64 and the results are mean values of 10 trials.

adequately satisfies the requirements of ECP monitoring. The observed evolution of inference costs aligns with the analytical results presented in Table V. One potential drawback of the SAMP module is its second-order complexity in relation to feature number D. However, this issue can be mitigated by mapping the input data into a lower-dimensional space before the SAMP block.

V. CONCLUSION

This study proposes a novel AttentionMixer framework to address the current limitations of ECP monitoring methods in terms of accuracy and interpretability, with the goal of providing a trustworthy process monitoring framework for ECPs operating under extreme conditions. The framework employs spatial and temporal adaptive message passing blocks to build a comprehensive representation of ECP logs. Additionally, a sparse message passing regularizer is utilized to eliminate spurious and noisy correlations. By explicitly modeling variate-wise correlations and effectively eliminating spurious correlations, AttentionMixer achieves better accuracy, interpretability, and therefore, trustworthiness in ECP monitoring. The evaluation of AttentionMixer on two real-world ECP monitoring datasets demonstrates its superior performance in terms of accuracy and interpretability, highlighting its potential to achieve trustworthy ECP monitoring.

The first direction aims to explore the role and flexibility of techniques in vanilla Transformers, such as patching [35], sparse attentions [36], [38], [57], and adversarial training [34], within the AttentionMixer framework, particularly in the SAMP block that is constructed based on variate-wise correlations. This exploration is expected to further improve the

monitoring quality of AttentionMixer. The second direction of our future work aims to deploy the proposed model on our online monitoring board¹ to serve nuclear power plants nationwide, which will enable us to evaluate the performance of the framework under a broader range of conditions and further refine its effectiveness.

REFERENCES

- [1] X. Wu, X.-H. Xia, G. Chen, X. Wu, and B. Chen, "Embodied energy analysis for coal-based power generation system-highlighting the role of indirect energy cost," *Appl. Energy*, vol. 184, pp. 936–950, 2016.
- [2] F.-C. Chen and M. R. Jahanshahi, "Nb-cnn: Deep learning-based crack detection using convolutional neural network and naïve bayes data fusion," *IEEE Trans. Ind. Electron.*, vol. 65, no. 5, pp. 4392–4400, 2018.
- [3] M. Embrechts and S. Benedek, "Hybrid identification of nuclear power plant transients with artificial neural networks," *IEEE Trans. Ind. Electron.*, vol. 51, no. 3, pp. 686–693, 2004.
- [4] H. Liu, Y. Wang, W. Fan, X. Liu, Y. Li, S. Jain, Y. Liu, A. Jain, and J. Tang, "Trustworthy ai: A computational perspective," *ACM Transactions on Intelligent Systems and Technology*, vol. 14, no. 1, pp. 1–59, 2022.
- [5] L. Floridi, "Establishing the rules for building trustworthy ai," *Nature Machine Intelligence*, vol. 1, no. 6, pp. 261–262, 2019.
- [6] W. Liang, G. A. Tadesse, D. Ho, L. Fei-Fei, M. Zaharia, C. Zhang, and J. Zou, "Advances, challenges and opportunities in creating data for trustworthy ai," *Nature Machine Intelligence*, vol. 4, no. 8, pp. 669–677, 2022.
- [7] A. F. Markus, J. A. Kors, and P. R. Rijnbeek, "The role of explainability in creating trustworthy artificial intelligence for health care: a comprehensive survey of the terminology, design choices, and evaluation strategies," *Journal of Biomedical Informatics*, vol. 113, p. 103655, 2021.
- [8] S. J. Nightingale and H. Farid, "Ai-synthesized faces are indistinguishable from real faces and more trustworthy," *Proceedings of the National Academy of Sciences*, vol. 119, no. 8, p. e2120481119, 2022.
- [9] R. Zelliers, A. Holtzman, H. Rashkin, Y. Bisk, A. Farhadi, F. Roesner, and Y. Choi, "Defending against neural fake news," *Advances in neural information processing systems*, vol. 32, 2019.
- [10] A. Sheth, M. Gaur, K. Roy, and K. Faldu, "Knowledge-intensive language understanding for explainable ai," *IEEE Internet Computing*, vol. 25, no. 5, pp. 19–24, 2021.
- [11] Y. Huang, H. Wang, Z. Liu, L. Pan, H. Li, and X. Liu, "Modeling task relationships in multi-variate soft sensor with balanced mixture-of-experts," *IEEE Trans. Ind. Informat.*, pp. 1–9, 2022.
- [12] X. Yuan, L. Li, and Y. Wang, "Nonlinear dynamic soft sensor modeling with supervised long short-term memory network," *IEEE Trans. Ind. Informat.*, vol. 16, no. 5, pp. 3168–3176, 2019.
- [13] X. Yuan, J. Zhou, B. Huang, Y. Wang, C. Yang, and W. Gui, "Hierarchical quality-relevant feature representation for soft sensor modeling: A novel deep learning strategy," *IEEE Trans. Ind. Informat.*, vol. 16, no. 6, pp. 3721–3730, 2019.
- [14] Q. Dai, C. Zhao, and B. Huang, "Incremental variational bayesian gaussian mixture model with incremental optimization for distribution accommodation and fine-scale adaptive process monitoring," *IEEE Trans. Cybern.*, 2022.
- [15] H. Wang, T. Chang, T. Liu, J. Huang, Z. Chen, C. Yu, R. Li, and W. Chu, "ESCM2: entire space counterfactual multi-task model for post-click conversion rate estimation," in *SIGIR*, pp. 363–372, ACM, 2022.
- [16] H. Li, W. Wang, Z. Liu, Y. Niu, H. Wang, S. Zhao, Y. Liao, W. Yang, and X. Liu, "A novel locality-sensitive hashing relational graph matching network for semantic textual similarity measurement," *Expert Systems with Applications*, vol. 207, p. 117832, 2022.
- [17] J. Fan, Y. Zhuang, Y. Liu, H. Jianye, B. Wang, J. Zhu, H. Wang, and S.-T. Xia, "Learnable behavior control: Breaking atari human world records via sample-efficient behavior selection," in *ICLR*, 2023.
- [18] A. Chandrakar, D. Datta, A. K. Nayak, and G. Vinod, "Statistical analysis of a time series relevant to passive systems of nuclear power plants," *Int. J. Syst. Assur. Eng. Manag.*, vol. 8, no. 1, pp. 89–108, 2017.
- [19] J. I. Aizpurua, S. D. J. McArthur, B. G. Stewart, B. Lambert, J. G. Cross, and V. M. Catterson, "Adaptive power transformer lifetime predictions through machine learning and uncertainty modeling in nuclear power plants," *IEEE Trans. Ind. Electron.*, vol. 66, no. 6, pp. 4726–4737, 2019.

- [20] L. Tang, L. Yu, S. Wang, J. Li, and S. Wang, "A novel hybrid ensemble learning paradigm for nuclear energy consumption forecasting," *Appl. Energy*, vol. 93, pp. 432–443, 2012.
- [21] H. Wang, M. Peng, R. Xu, A. Ayodeji, and H. Xia, "Remaining useful life prediction based on improved temporal convolutional network for nuclear power plant valves," *Front. Energy Res.*, vol. 8, p. 296, 2020.
- [22] Z. Wu, S. Pan, G. Long, J. Jiang, and C. Zhang, "Graph wavenet for deep spatial-temporal graph modeling," in *IJCAI*, pp. 1907–1913, 2019.
- [23] Z. Wu, S. Pan, G. Long, J. Jiang, X. Chang, and C. Zhang, "Connecting the Dots: Multivariate Time Series Forecasting with Graph Neural Networks," in *SIGKDD*, pp. 753–763, 2020.
- [24] Z. Chen and Z. Ge, "Knowledge automation through graph mining, convolution and explanation framework: a soft sensor practice," *IEEE Trans. Ind. Informat.*, 2021.
- [25] Z. Liu, Y. Lin, Y. Cao, H. Hu, Y. Wei, Z. Zhang, S. Lin, and B. Guo, "Swin transformer: Hierarchical vision transformer using shifted windows," in *ICCV*, pp. 10012–10022, 2021.
- [26] J. Jumper, R. Evans, A. Pritzel, T. Green, M. Figurnov, O. Ronneberger, K. Tunyasuvunakool, R. Bates, *et al.*, "Highly accurate protein structure prediction with alphafold," *Nature*, vol. 596, no. 7873, pp. 583–589, 2021.
- [27] Y. Ma and J. Tang, *Deep Learning on Graphs*. Cambridge University Press, 2021.
- [28] A. Vaswani, N. Shazeer, N. Parmar, J. Uszkoreit, L. Jones, A. N. Gomez, L. Kaiser, and I. Polosukhin, "Attention is all you need," *NeurIPS*, vol. 30, 2017.
- [29] T. Zhou, Z. Ma, Q. Wen, X. Wang, L. Sun, and R. Jin, "Fedformer: Frequency enhanced decomposed transformer for long-term series forecasting," in *ICML*, pp. 27268–27286, PMLR, 2022.
- [30] H. Zhou, S. Zhang, J. Peng, S. Zhang, J. Li, H. Xiong, and W. Zhang, "Informer: Beyond efficient transformer for long sequence time-series forecasting," in *AAAI*, vol. 35, pp. 11106–11115, 2021.
- [31] S. Liu, H. Yu, C. Liao, J. Li, W. Lin, A. X. Liu, and S. Dustdar, "Pyraformer: Low-complexity pyramidal attention for long-range time series modeling and forecasting," in *International conference on learning representations*, 2021.
- [32] S. Li, X. Jin, Y. Xuan, X. Zhou, W. Chen, Y.-X. Wang, and X. Yan, "Enhancing the locality and breaking the memory bottleneck of transformer on time series forecasting," *Advances in neural information processing systems*, vol. 32, 2019.
- [33] L. Shen and Y. Wang, "Tect: Tightly-coupled convolutional transformer on time series forecasting," *Neurocomputing*, vol. 480, pp. 131–145, 2022.
- [34] S. Wu, X. Xiao, Q. Ding, P. Zhao, Y. Wei, and J. Huang, "Adversarial sparse transformer for time series forecasting," *NeurIPS*, vol. 33, pp. 17105–17115, 2020.
- [35] Y. Nie, N. H. Nguyen, P. Sinthong, and J. Kalagnanam, "A time series is worth 64 words: Long-term forecasting with transformers," in *ICLR*, 2023.
- [36] N. Kitaev, L. Kaiser, and A. Levskaya, "Reformer: The efficient transformer," in *ICLR*.
- [37] M. Zaheer, G. Guruganesh, K. A. Dubey, J. Ainslie, C. Alberti, S. Ontaño, P. Pham, A. Ravula, Q. Wang, L. Yang, and A. Ahmed, "Big bird: Transformers for longer sequences," in *NeurIPS*, vol. 33, pp. 17283–17297, 2020.
- [38] K. M. Choromanski, V. Likhoshesterov, D. Dohan, X. Song, A. Gane, T. Sarlos, P. Hawkins, J. Q. Davis, A. Mohiuddin, L. Kaiser, *et al.*, "Rethinking attention with performers," in *ICLR*.
- [39] S. Wu, X. Xiao, Q. Ding, P. Zhao, Y. Wei, and J. Huang, "Adversarial
- [40] K. Champion, B. Lusch, J. N. Kutz, and S. L. Brunton, "Data-driven discovery of coordinates and governing equations," *PNAS*, vol. 116, no. 45, pp. 22445–22451, 2019.
- [41] Z. Wu, S. Pan, G. Long, J. Jiang, X. Chang, and C. Zhang, "Connecting the dots: Multivariate time series forecasting with graph neural networks," in *SIGKDD*, pp. 753–763, 2020.
- [42] P. Ball *et al.*, "The start-ups chasing clean, carbon-free fusion energy," *Nature*, vol. 599, no. 7885, pp. 362–366, 2021.
- [43] R. Y. Cui, N. Hultman, D. Cui, H. McJeon, S. Yu, M. R. Edwards, A. Sen, K. Song, C. Bowman, L. Clarke, *et al.*, "A plant-by-plant strategy for high-ambition coal power phaseout in china," *Nat. Commun.*, vol. 12, no. 1, pp. 1–10, 2021.
- [44] L. Li, A. J. Blomberg, J. D. Spengler, B. A. Coull, J. D. Schwartz, and P. Koutrakis, "Unconventional oil and gas development and ambient particle radioactivity," *Nat. Commun.*, vol. 11, no. 1, pp. 1–8, 2020.
- [45] C. Liu, W. Zhang, K. Ungar, E. Korpach, B. White, M. Benotto, and E. Pellerin, "Development of a national cosmic-ray dose monitoring system with health canada's fixed point surveillance network," *J. Environ. Radioact.*, vol. 190, pp. 31–38, 2018.
- [46] Y.-J. Huang, Z.-H. Shang-Guan, F. Zhao, M.-G. Lin, X.-D. Sha, D.-Y. Luo, Q. Chen, and K. Peng, "A correlation study of continuously monitored gamma dose rate and meteorological conditions," *J. Environ. Radioact.*, vol. 192, pp. 467–477, 2018.
- [47] J. Hirouchi, S. Hirao, J. Moriizumi, H. Yamazawa, and A. Suzuki, "Estimation of infiltration and surface run-off characteristics of radionuclides from gamma dose rate change after rain," *J. Nucl. Sci. Technol.*, vol. 51, no. 1, pp. 48–55, 2014.
- [48] J. F. Mercier, B. L. Tracy, R. D'Amours, F. Chagnon, I. Hoffman, E. P. Korpach, S. Johnson, and R. K. Ungar, "Increased environmental gamma-ray dose rate during precipitation: a strong correlation with contributing air mass," *J. Environ. Radioact.*, vol. 100, no. 7, pp. 527–533, 2009.
- [49] M. Kowatari, H. Yoshitomi, S. Nishino, Y. Tanimura, T. Ohishi, P. Kessler, S. Neumaier, and A. Röttger, "Establishment of a Low Dose Rate Gamma Ray Calibration Field for Environmental Radiation Monitoring Devices," *Radiat. Prot. Dosimetry.*, pp. 1–8, 2019.
- [50] Y. K. Chan and Y. C. Tsai, "Multiple regression approach to predict turbine-generator output for Chinshan nuclear power plant," *Kerntechnik*, vol. 82, no. 1, pp. 24–30, 2017.
- [51] S. Grape, E. Branger, Z. Elter, and L. P. Balkesthäl, "Determination of spent nuclear fuel parameters using modelled signatures from non-destructive assay and random forest regression," *Nucl. Instrum. Methods Phys. Res., Sect. A*, vol. 969, p. 163979, 2020.
- [52] J. Choi and S. J. Lee, "Consistency Index-Based Sensor Fault Detection System for Nuclear Power Plant Emergency Situations Using an LSTM Network," *Sensors*, vol. 20, no. 6, p. 1651, 2020.
- [53] J. Zhang, Z. Pan, W. Bai, and X. Zhou, "Pressurizer water level reconstruction for nuclear power plant based on gru," in *IMCCC*, pp. 1675–1679, 2018.
- [54] D. P. Kingma and J. A. Ba, "Adam: A method for stochastic optimization," in *ICLR*, vol. 434, pp. 1–15, 2015.
- [55] T. M. Nguyen, V. Suliafu, S. J. Osher, L. Chen, and B. Wang, "Fmm-former: Efficient and flexible transformer via decomposed near-field and far-field attention," in *NeurIPS*, vol. 34, pp. 29449–29463, 2021.
- [56] M. Zaheer, G. Guruganesh, K. A. Dubey, J. Ainslie, C. Alberti, S. Ontanon, P. Pham, A. Ravula, Q. Wang, L. Yang, *et al.*, "Big bird: Transformers for longer sequences," *Advances in neural information processing systems*, vol. 33, pp. 17283–17297, 2020.
- [44] M. B. Roth and P. Jaramillo, "Going nuclear for climate mitigation: An analysis of the cost effectiveness of preserving existing us nuclear power plants as a carbon avoidance strategy," *Energy*, vol. 131, pp. 67–77, 2017.